Progress in Nuclear Energy 64 (2013) 31–40

Contents lists available at SciVerse ScienceDirect

Progress in Nuclear Energy

journal homepage: www.elsevier.com/locate/pnucene

Two-dimensional numerical simulation of single bubble rising behavior in liquid metal using moving particle semi-implicit method

Juanli Zuo, Wenxi Tian*, Ronghua Chen, Suizheng Qiu*, Guanghui Su

School of Nuclear Science and Technology, State Key Laboratory of Multiphase Flow in Power Engineering, Xi'an Jiao Tong University, No. 28, Xianning West Road, Xi'an 710049, China

ARTICLE INFO

Article history:
Received 10 December 2011
Received in revised form
18 December 2012
Accepted 19 December 2012

Keywords:
Two phase flow
MPS method
Bubble shape
Terminal velocity
Aspect ratio
Fundamental research

ABSTRACT

Gas-lift pump in liquid metal cooling fast reactor (LMFR) is an innovative conceptual design to enhance the natural circulation ability of reactor core. The two phase flow characteristics of gas–liquid metal make significant improvement of the natural circulation capacity and reactor safety. It is important to study bubble flow in liquid metal. In present study, the rising behaviors of a single nitrogen bubble in 5 kinds of common stagnant liquid metals (lead bismuth alloy (LBE), liquid kalium (K), sodium (Na), potassium sodium alloy (Na–K) and lithium lead alloy (Li–Pb)) and in flowing lead bismuth alloy have been numerically simulated using two-dimensional moving particle semi-implicit (MPS) method. The whole bubble rising process in liquid was captured. The bubble shape, rising velocity and aspect ratio during rising process of single nitrogen bubble were studied. The computational results show that, in the stagnant liquid metals, the bubble rising shape can be described by the Grace's diagram, the terminal velocity is not beyond 0.3 m/s, the terminal aspect ratio is between 0.5 and 0.6. In the flowing lead bismuth alloy, as the liquid velocity increases, both the bubble aspect ratio and terminal velocity increase as well. This work is the fundamental research of two phase flow and will be important to the study of the natural circulation capability of Accelerator Driven System (ADS) by using gas-lift pump.

1. Introduction

In the conceptual design of liquid metal cooling fast reactor and the Accelerator Driven System (ADS), the traditional mechanical pump in primary coolant circuit was replaced by gas-lift pump (Cinotti and Gherardi, 2002). Fig. 1 shows lead bismuth cooling ADS device (PDS-XADS) scheme (Tohru et al., 2005), the subcritical reactor was cooled by lead bismuth natural cycle without primary circuit pump. The two phase flow of LBE-inert gas in ascension channel could significantly improve natural circulation capacity. Russia also adopts gas-lift pump in their conceptual design of 900 MWt lead bismuth cooling fast reactor (RBEC-M) (Mikityuk et al., 2002). The two-phase flow characteristics of LBE-inert gas have obviously influence on the natural cycle of system ability and reactor safety. However, there are few studies on the bubble flow in liquid metal, and it is difficult to obtain the visualization of bubble rising process in liquid metal. Consequently, it is of great significance to numerically simulate the two-phase flow characteristics.

The finite difference method (FDM), finite volume method (FVM) and finite element method (FEM), are common traditional mesh-based methods. In these methods, because of the severe distortion of computing cells near two-phase interface, the accurate configuration of movable interface is too much complicated or even difficult. The computational efficiency is also very low and computation sometimes fails. So other novel methods appeared to overcome these disadvantages, such as the moving grid method, the front tracking method (Unverdi and Tryggvason, 1992), the level set method (Smereka and Sethian, 2003), the volume-of-fluid method (VOF) (Scardovelli and Zaleski, 1999), and the boundary-integral algorithm (Dhotre and Smith, 2007). Among them, moving particle semi-implicit (MPS) method, proposed by Koshizuka and Oka (1996) is one promising particle method, which is on the basis of smoothed particle hydrodynamics (SPH). Comparing with the above methods, MPS method has the following distinguished features. Interface tracing technique is its inherent feature for different fluid or phase which can be represented by different type of particles, so interface can be easily captured and its resolution accuracy scales with particle size. No additional governing equation for tracing interface is needed. Principally, it can be used to treat arbitrary deformation and easier to implement.

Compared with 3D, 2D simulation of MPS method is possible to perform the bubble rising behavior, and the calculation results of

* Corresponding authors. Tel./fax: +86 29 82665607.
E-mail addresses: wxtian@mail.xjtu.edu.cn (W. Tian), szqiu@mail.xjtu.edu.cn (S. Qiu).

0149-1970/$ – see front matter © 2012 Elsevier Ltd. All rights reserved.
http://dx.doi.org/10.1016/j.pnucene.2012.12.003

Nomenclature

C_D	drag coefficient
D	bubble diameter (m)
d	space dimension
d_{eq}	bubble equivalent diameter (m)
E	bubble aspect ration
E_0	Eotvos number
g	gravity acceleration (m/s^2)
k	steam liquid interface curvature (m^{-1})
M	Morton number
$\mathbf{n}$	unite vector of phase interface
n	particle density
p	pressure (Pa)
$\mathbf{r}$	particle location vector
r_e	particle effective radius (m)
Re	Reynolds number
t	time (s)
T	temperature (K)
$\mathbf{u}$	particle velocity vector
u_{gu}	terminal rising velocity of bubble (m/s)
w	kernel function

Greek symbols

φ	scalar variable
λ	diffusion model parameter
μ	kinematic viscosity (kg/ms)
ρ	density (kg/m^3)
σ	surface tension coefficient

Superscript/subscript

f	liquid
g	gas
i,j	particle no

2D are similar to that of 3D simulation. So in present study, the bubble flow characteristics of a single inert gas bubble in five kinds of stagnant liquid metals and flowing lead bismuth alloy were studied by two dimensional MPS method. In the process of bubble rising, the deformation of bubble shape, the rising velocity and the aspect ratio were analyzed, and the numerical simulation results were compared with Grace's diagram and empirical correlations.

2. Numerical method and calculation procedure

MPS method described by Lagrangian method, does not have the discrete convective term which may cause numerical dissipation. The differential operator in the fluid control equation is replaced by the particle interaction model using the kernel function. The incompressible characteristic of fluid is realized by keeping a constant particle density number in flow field. The momentum equations and pressure term are solved using semi-implicit method and implicit method, respectively. The other terms are solved using explicit method.

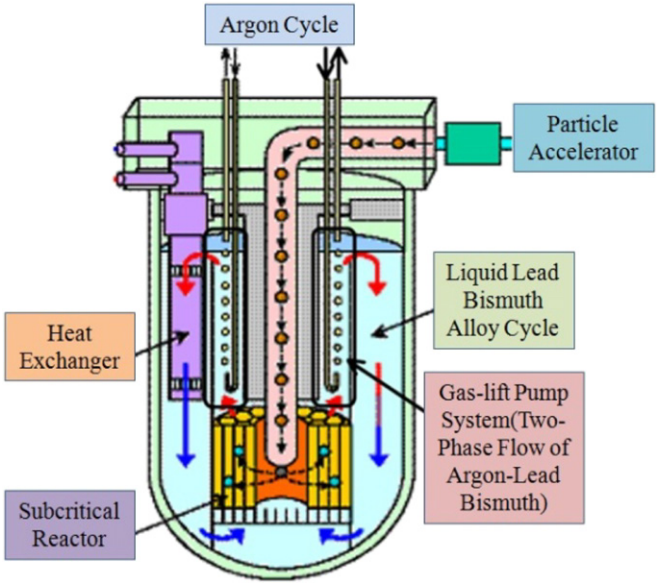

Fig. 1. ADS schematic.

2.1. Control equation

The continuity, Navier–Stokes and energy equations for incompressible viscous flows are:

$$\nabla\cdot\mathbf{u}=0 \tag{1}$$

$$\rho\left(\frac{\partial\mathbf{u}}{\partial t}+(\mathbf{u}-\mathbf{u}^c)\cdot\nabla\mathbf{u}\right)=-\nabla p+\mu\nabla^2\mathbf{u}+\sigma\kappa\cdot\mathbf{n}+\rho\mathbf{g} \tag{2}$$

Where, $\mathbf{u}$ is the fluid velocity and $\mathbf{u}^c$ represents the motion of a computing point which is adaptively configures during the calculation. κ is curvature of the interface, which is calculated in the surface tension function of MPS method. An arbitrary calculation is allowed between fully Lagrangian ($\mathbf{u}^c=\mathbf{u}$) and Eulerian ($\mathbf{u}^c=0$) calculations so that a sharp fluid front is calculated accurately by moving the computing points in Lagrangian coordinates while the fixed boundaries are described with Eulerian coordinates (Yoon et al., 1999).

2.2. Numerical method

In MPS method, each differential operator appeared in the governing equations is replaced by the particle interaction models where a particle interacts with others in its vicinity covered with a weight function $w(r,r_e)$, where r is the distance between two particles and r_e is the radius of interaction area. There are several kernel function expressions proposed by different researchers. Among them, Koshizuka's equation has been widely adopted since it has simple expression and reasonable physical meaning. So Koshizuka's kernel function has been proposed in the study (Koshizuka and Oka, 1996).

$$w(r,r_e)=\begin{cases}\dfrac{r_e}{r}-1 & (0\le r\le r_e)\\ 0 & (r_e\le r)\end{cases} \tag{3}$$

Since the area that is covered with this weight function is bounded, a particle interacts with a finite number of neighboring particles as shown in Fig. 2 (Tian et al., 2009).

The particle distribution in the flow field is evaluated by particle number density in MPS method. The particle number density of i in the position r_i is defined by:

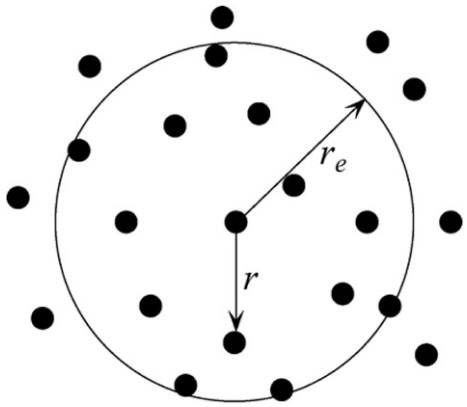

Fig. 2. Schematic diagram of particle effective radius.

$$n_i = \sum_{j \neq i} w(|\mathbf{r}_j - \mathbf{r}_i|) \tag{4}$$

The particle number density is proportional to the fluid density. It should be constant for incompressible flow: $n_i = n^0$, where n^0 is dependent on the initial arrangement of particles (Duan et al., 2003).

$$n^0 = \sum_{j \neq i} w(|\mathbf{r}_j^0 - \mathbf{r}_i^0|) \tag{5}$$

Besides these, particle interaction models, including gradient model, divergence model and Laplacian model, are prepared for the differential operator appeared in the governing equations. The gradient and Laplacian of physical quantity Φ on particle i are expressed by the summation of physical quantities Φ over its neighboring particles j according to a kernel function w as.

Gradient model:

$$(\nabla\phi)_i = \frac{d}{n_i} \sum_{j \neq i} \left[\frac{\phi_j - \phi_i}{|\mathbf{r}_j - \mathbf{r}_i|^2} (\mathbf{r}_j - \mathbf{r}_i) w(|\mathbf{r}_j - \mathbf{r}_i|) \right] \tag{6}$$

Laplace model:

$$\left(\nabla^2\phi\right)_i = \frac{2d}{\lambda n_i} \sum_{j \neq i} \left[\left(\phi_j - \phi_i\right) w(|\mathbf{r}_j - \mathbf{r}_i|) \right] \tag{7}$$

Where λ is the diffusion coefficient in MPS method and can be determined as

$$\lambda_i = \frac{\sum_{j \neq i} \left[w(|\mathbf{r}_j - \mathbf{r}_i|) |\mathbf{r}_j - \mathbf{r}_i|^2 \right]}{\sum_{j \neq i} \left[w(|\mathbf{r}_j - \mathbf{r}_i|) \right]} \tag{8}$$

The divergence operator is modeled just like the same way in the gradient, since it is a scalar product of gradient vectors. The velocity divergence between two particles i and j is defined by $(\mathbf{u}_j - \mathbf{u}_i)(\mathbf{r}_j - \mathbf{r}_i)/|(\mathbf{r}_j - \mathbf{r}_i)|^2$ and the velocity divergence at the particle i is given by the weighted average of the individual velocity divergences.

Divergence model:

$$(\nabla \cdot \mathbf{u})_i = \frac{d}{n_i} \sum_{j \neq i} \left[\frac{(\mathbf{u}_j - \mathbf{u}_i) \cdot (\mathbf{r}_j - \mathbf{r}_i)}{|\mathbf{r}_j - \mathbf{r}_i|^2} w(|\mathbf{r}_j - \mathbf{r}_i|) \right] \tag{9}$$

For the analysis of two-phase interface problems where the curvature of the interface is large, a calculation model for the surface tension force is used. In general, the pressure difference Δp between gas and liquid is

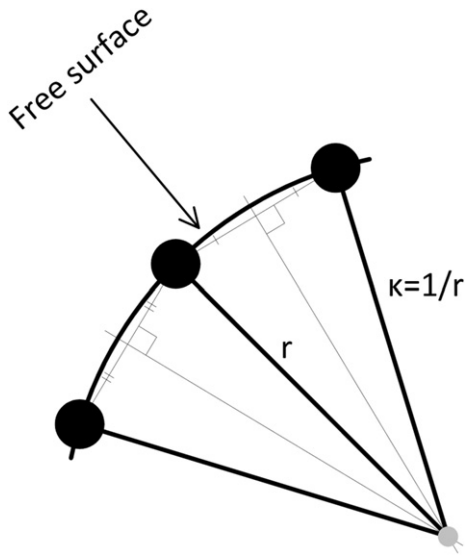

Fig. 3. Illustration for determination of curvature of curvilinear surface.

$$\Delta p = \sigma\kappa \tag{10}$$

Where σ is surface tension coefficient and κ is the interface curvature.

In the present study, a continuous curvilinear surface is obtained by connecting the computing points on phase interface. Then the curvature κ is calculated from the radius of circumference whose center is determined to be the intersection points of two perpendicular bisectors. It is shown in Fig. 3 (Heo et al., 2002). This model is verified through the calculation of volume decrease of a gas bubble in stagnant liquid due to surface tension.

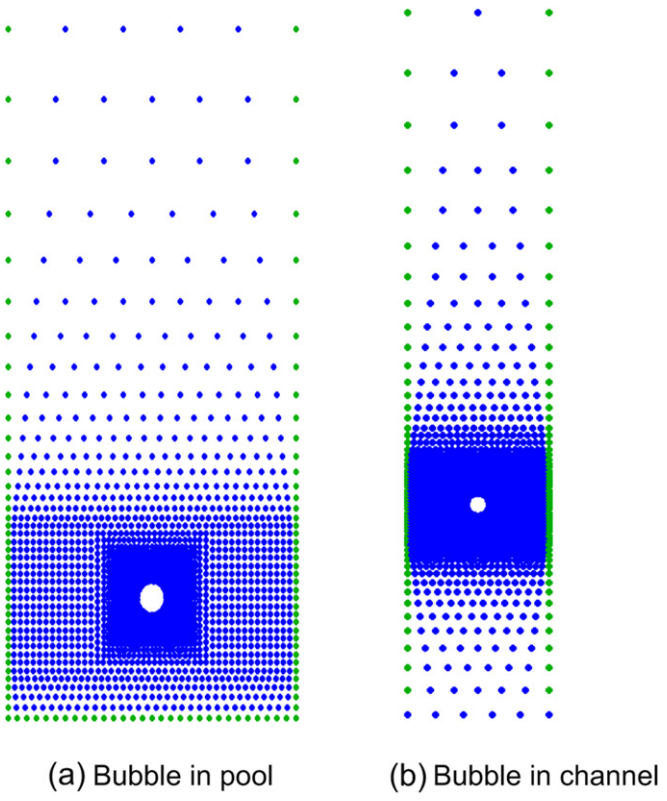

Fig. 4. Computational domain and boundary (a) bubble in pool (b) bubble in channel.

2.3. The computational domain and boundary condition

Two-dimensional particle models were constructed for a single spherical bubble rising under buoyancy in the quiescent liquid pool and the flowing liquid channel, as shown in Fig. 4. The model consisted of fluid particles for liquid metal and rigid particles for the wall. The initial inert gas bubble was located in the calculation area. The distance between the bubble center and the wall was set to be larger than five times of the bubble radius to eliminate the effects of the wall (Tian et al., 2010). The computational domain height should be large enough to make sure that the bubble can reach the terminal velocity and stable shape. Thus, in this study the pool area is 0.1 m in width, 0.2 m in height, the channel area is 0.1 m in width, 0.5 m in height. The liquid was described using discretized particles with non-uniform scheme. The particle size (distance between adjacent particles) decreased with the increase of the axial distance away from the center. The topology structure of gas–liquid interface is described by moving particle position.

As a boundary condition, in Fig. 4(a), both lateral and bottom walls are set to be rigid insulated boundaries and the top is free surface boundary, in Fig. 4(b), the lateral wall is set to be rigid insulated boundary, the top and the bottom are free surface boundaries. The pressure in the bubble is calculated from gas state equation.

2.4. Flow chart

Semi-implicit time stepping method is used in MPS method. In each layer, the initial estimated values of particle velocity and position are obtained firstly by calculating the viscous term and source term in momentum conservation equation using explicit formulation; then, modified value of particle velocity and position are obtained by solving the mass conservation equation using implicit formulation; finally, the particle velocity and position values of the next layer are obtained. The programming flow chart is shown in Fig. 5. Incomplete Cholesky Conjugate Gradient (ICCG) is an effective method for solving large-scale symmetric positive definite sparse matrix equations. ICCG algorithm is the improved Conjugate Gradient (CG) method. In order to overcome the disadvantage of slow iterative of CG under large coefficient matrix condition, we

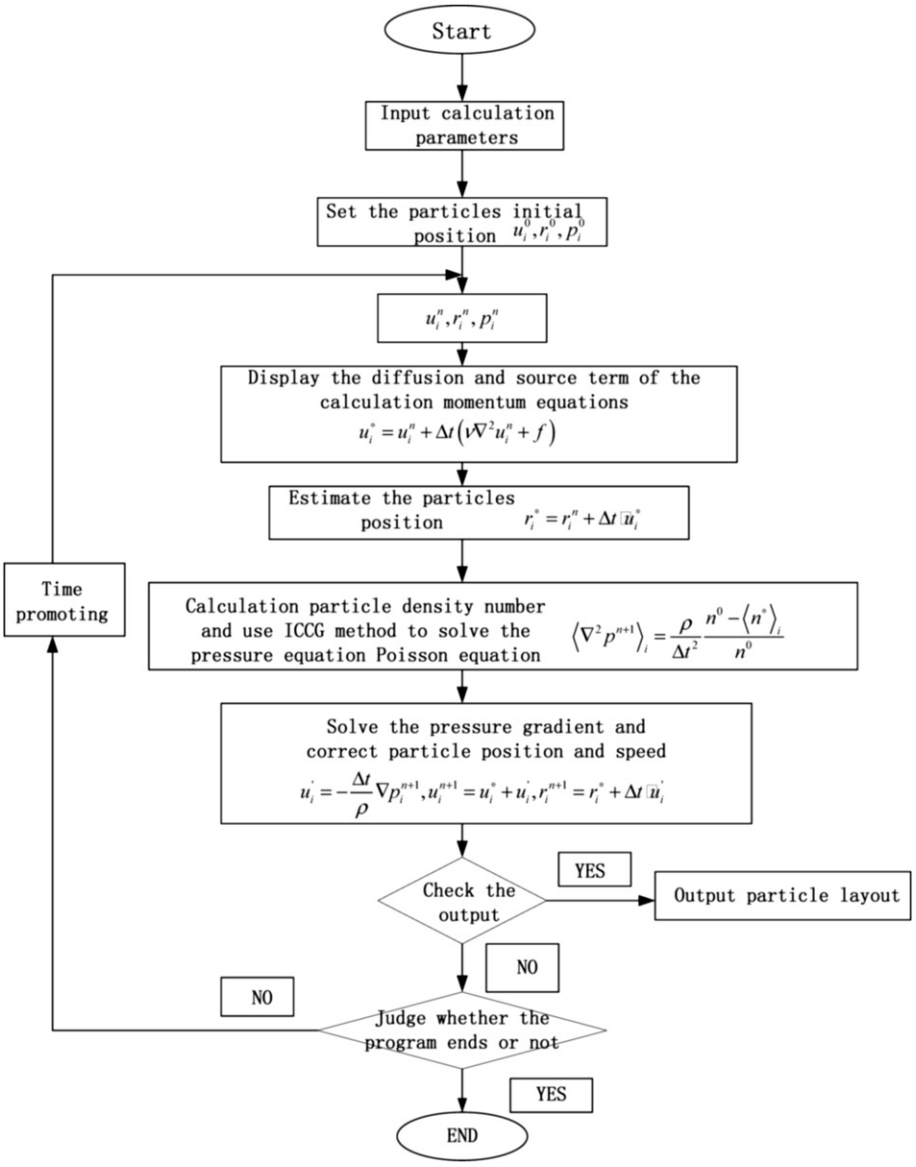

Fig. 5. The flow chart of MPS method.

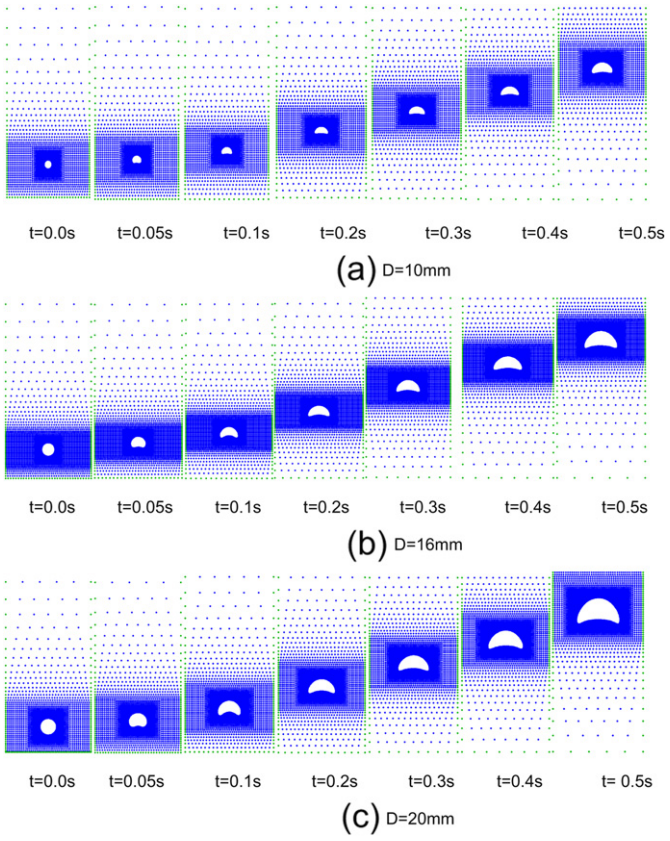

Fig. 6. The bubble rising process in lead bismuth with different initial diameters (a) $D = 10$ mm, (b) $D = 16$ mm, (c) $D = 20$ mm.

pretreatment the coefficient matrix and put forward a series of pretreatment conjugate gradient method.

3. Results and analysis

3.1. The bubble rising process in stagnant lead bismuth alloy with different initial bubble diameters

The rising behaviors of the single nitrogen gas bubble in lead bismuth alloy (56.5% Bi, 200 °C) are shown in Fig. 6. In Fig. 6(a), the initial bubble diameter is 10 mm. At 0.005 s, the bottom of the initial spherical bubble pits upward, and extends crosswise. At 0.3 s, the bubble shape is hemisphere, then the bottom of this bubble pits upward continually, at 0.5 s, is similar to a spherical cap. In Fig. 6(b), the initial bubble diameter is 16 mm. At start, it changes to dimples shape, then develops crosswise, finally becomes spherical cap. During the 0.5 s, the rising distance of the bubble with an initial diameter at 16 mm is larger than that with an initial diameter at 10 mm. As shown in Fig. 6(c), the initial bubble diameter is 20 mm, the changing trend is similar to the former situation, except the shape of bubble is a little larger.

The volume of the gas increases as it rises in the liquid due to the decrease in the hydraulic pressure. So, in the bubble rising process, the bubble equivalent diameter d_{eq} increases with rising time. In Fig. 7, it shows the change of d_{eq} when initial bubble diameter is 10 mm.

Table 1
Coefficients in Eq. (15).

A_1	A_2	A_3	m	Ref.	Remarks
24	0	0	0	(Schlichting, 1979)	Classical Stokes' law, rigid sphere, Re < 1
24	0	0	0.188	(Schlichting, 1979)	Oosen solution, rigid sphere, Re < 5
24	3.6	0	0.313	(Clift et al., 1978)	Schiller and Nauman, rigid sphere, Re < 800
48	0	0	0	(Levich, 1972)	Levich, pure system, Re > 100
48	−106.1	0	1.5	(Clift et al., 1978)	Moore, pure system, 20 < Re < 1000
72	0	0	0	(Tomiyama et al., 1998)	Levich, slightly cont. system
24	2.4	0	0.25	(Tomiyama et al., 1998)	Ishii and Chawla
0	18.7	0	0.68	(Peebles and Garber, 1953)	Peebles and Garber

Table 2
Bubble rising parameter in lead bismuth alloy.

D (mm)	M	E_0	Re	Empirical correlation-u_{gu} (m/s)
10	9.5×10^{-13}	30	9.26×10^3	0.221
16	9.5×10^{-13}	76.06	1.71×10^4	0.28
20	9.5×10^{-13}	118.84	2.26×10^4	0.31

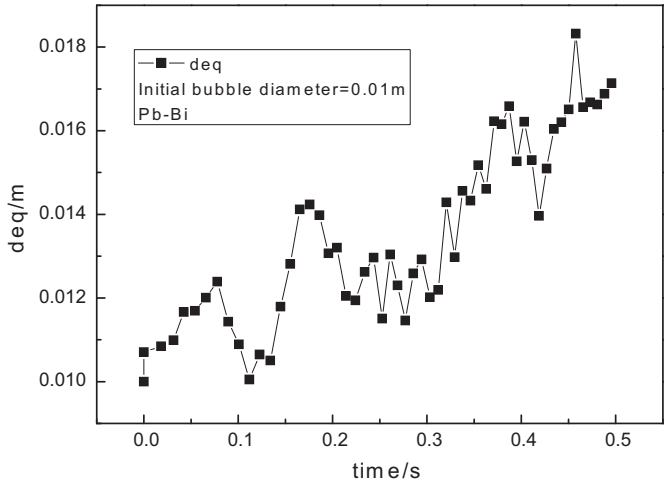

Fig. 7. The bubble equivalent diameter in lead bismuth.

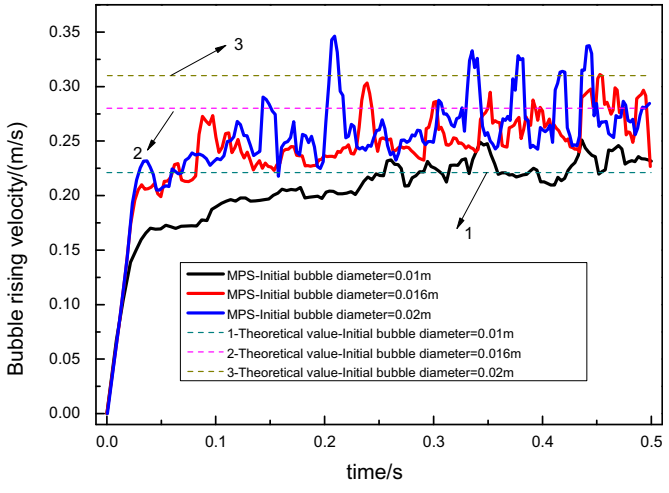

Fig. 8. The bubble rising velocity in lead–bismuth.

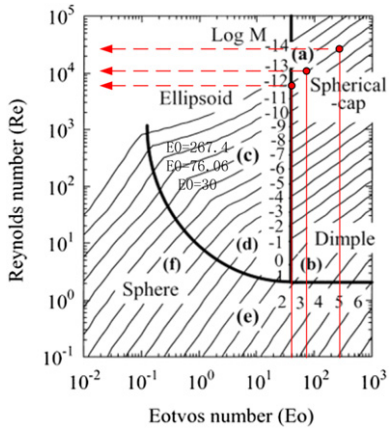

Fig. 9. The comparison between the simulation and Grace's diagram with 3 different initial diameters.

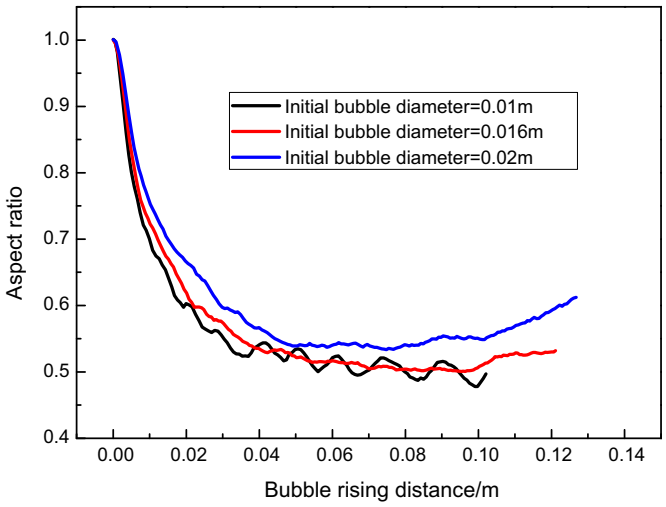

Fig. 10. The change of aspect ratio in different initial bubble diameters.

There are many studies on bubble adiabatic upflow characteristics in viscous fluid. There exist a lot of factors influencing bubble rising behavior, such as surface tension, fluid viscosity, inertia, buoyancy and friction. The shapes of bubbles are categorized by using three dimensionless numbers: Morton, Eotvos and Reynolds. These dimensionless numbers are defined as (Suzuki et al., 2003)

$$\mathrm{Re} = \left(\rho_f u_g d_{\mathrm{eq}}\right)\Big/\mu_f \tag{11}$$

$$Eo = g\left(\rho_f - \rho_g\right)d_{\mathrm{eq}}^2/\sigma \tag{12}$$

$$M = \left(g\mu_f^4\right)\left(\rho_f - \rho_g\right)\Big/\left(\rho_f^2\sigma^3\right) \tag{13}$$

The bubble velocity is defined as the change rate of the position at the center of largest vertical bubble cross-section with time. As the bubble shape during the rising process simultaneously changes in vertical and horizontal directions, there are fluctuations on the calculated velocity curve. In the bubble rising process, the terminal rising velocity of the bubble, u_{gu}, is defined as the bubble rising velocity after the bubble is stable, which is a key parameter to character the bubble flow in liquid. The terminal velocity of the bubble can be derived as (Marco et al., 2003).

$$u_{gu} = \sqrt{\frac{4\left(\rho_f - \rho_g\right)g d_{\mathrm{eq}}}{3C_D\rho_f}} \tag{14}$$

When $Eo \le 0.25$,

$$C_D = \frac{A_1}{\mathrm{Re}} + \frac{A_2}{\mathrm{Re}^m} + A_3 \tag{15}$$

Some of the proposed coefficients are reported in Table 1.
When $0.25 < Eo < 40$,

$$C_D = \frac{2}{3}\sqrt{Eo}(Eo < 16) \quad C_D = \frac{8}{3}(Eo \ge 16) \tag{16}$$

$$\text{or} \quad C_D = \frac{8}{3}\frac{Eo}{Eo+4}, \tag{17}$$

When $Eo \ge 40$,

$$C_D = 3\frac{d_{\mathrm{eq}}}{r} \tag{18}$$

Since for Re > 150 the bubble becomes a spherical cap with a wake angle of approximately 50° (Clift et al., 1978), after some manipulation $d_{\mathrm{eq}}/r \cong 0.89$ is found, which gives $C_D = 8/3$.

The Morton, Eotvos and Reynolds numbers of the bubble with three different initial diameters and the u_{gu} calculated by the empirical correlations in lead bismuth alloy are shown in Table 2.

The bubble rising velocities with bubble rising time are shown in Fig. 8. In MPS calculation, when the initial bubble diameter is 10 mm, 16 mm and 20 mm, their rising velocity changing trend is similar. In first 0.03 s, the velocity rapidly increases. Then the increase of rising velocity is slow and with large fluctuations. At last, it will reach the terminal rising velocity. In the figure, the three dotted lines represent the terminal velocity calculated by empirical correlations. We can see that the u_{gu} calculated by MPS has a little

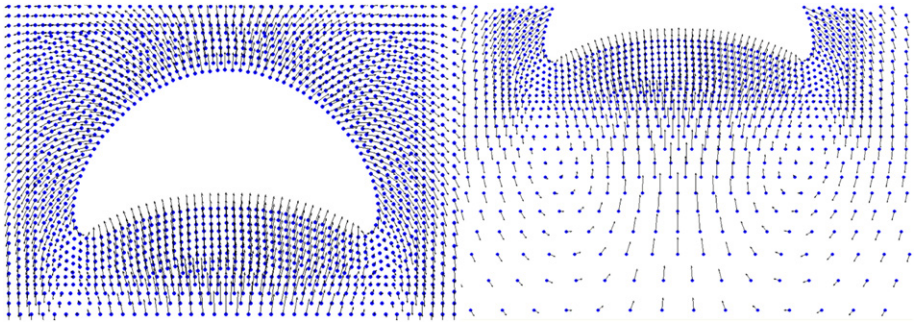

Fig. 11. The bubble velocity field (D = 10 mm) in lead bismuth alloy.

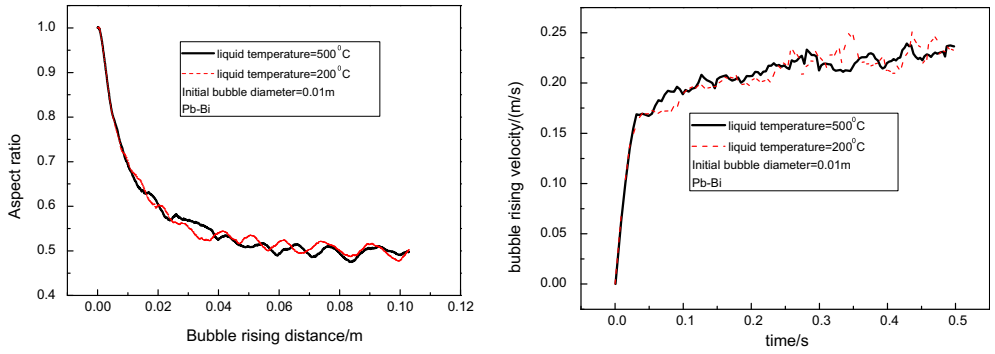

Fig. 12. The change of aspect ratio and bubble rising velocity in different liquid temperature.

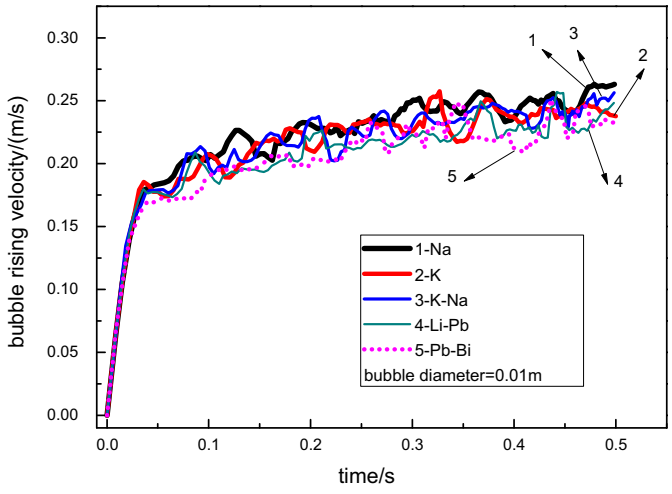

Fig. 13. The bubble rising velocity in different liquid metals.

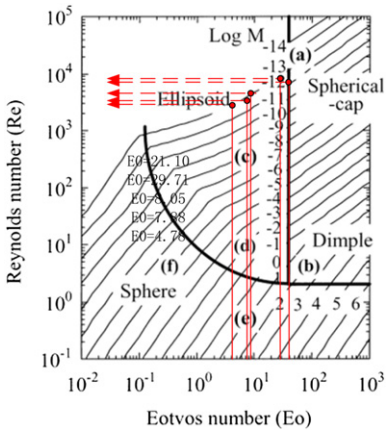

Fig. 14. The comparison between the simulation and Grace's diagram in 5 different liquid metals.

difference from the theoretical values and the terminal rising velocity increases with initial bubble diameter.

Grace (1973, 1976) and Clift et al. (1978) summarized available experimental data and proposed the well known graphical correlation as shown in Fig. 9, in which Morton and Eotvos numbers were adopted to determine the stable shape of a single rising bubble in an infinite stagnant liquid. Grace's correlation is only valid for evaluating the final stable state of immiscible bubble flow. Comparison between the calculated bubble shapes and Grace's graphical correlation indicates that all transient bubble shapes can be found in Grace's graphical correlation.

From Fig. 9, we find that, in these three cases, the ultimate shape of bubble is spherical cap. When the bubble terminal rising velocity by MPS method is determined, the calculated Re is almost in accordance with the Re in Grace's graphical correlation chart.

Besides the terminal velocity, another important parameter is aspect ratio-E (Celata et al., 2007), which is the ratio of the minor to the major axis of the bubble. As shown in Fig. 10, the change of aspect ratio with bubble rising distance in different initial bubble diameters, is reported. When the bubble is rising, the aspect ratio decreases rapidly from 1.0 to the value around 0.5–0.6. And when the initial bubble diameter is larger, the aspect ratio increases with small scale.

Fig. 11 shows the velocity field around the bubble in lead-bismuth alloy when bubble initial diameter is 10 mm. The wake flow is formed during the bubble rising process. Because of the bubble deformation, there will be two eddy structures on both sides of the bubble. The wake flow and eddy will make significantly influence on the bubble flow character in liquid metal, which is in close relation to the natural circulation ability.

Fig. 12 shows the change of aspect ratio and bubble rising velocity with initial bubble diameter 10 mm, when the liquid temperature is 500 °C, 200 °C, respectively. In MPS method, the fluid temperature has little influence on the parameters, such as aspect ratio and bubble rising velocity.

Table 3
The parameters in different kinds of liquid metals.

Liquid–gas	σ	ρ	μ	M (bubble)	E_0 (bubble)	Re (bubble)
Na	185.0×10^{-3}	903.56	4.57×10^{-4}	7.47×10^{-14}	4.78	4.74×10^{3}
Na–K	103.0×10^{-3}	828.0	3.74×10^{-4}	2.12×10^{-13}	7.88	5.31×10^{3}
K	95.25×10^{-3}	783.0	3.01×10^{-4}	1.20×10^{-13}	8.05	5.97×10^{3}
Li–Pb	456.97×10^{-3}	9838.0	2.15×10^{-3}	2.24×10^{-13}	21.10	1.68×10^{4}
LBE	346.0×10^{-3}	10,490.0	2.55×10^{-3}	9.52×10^{-13}	29.71	9.26×10^{3}
N_2 (200 °C)	/	0.711	2.51×10^{-5}	/	/	/
N_2 (300 °C)	/	0.588	2.51×10^{-5}	/	/	/

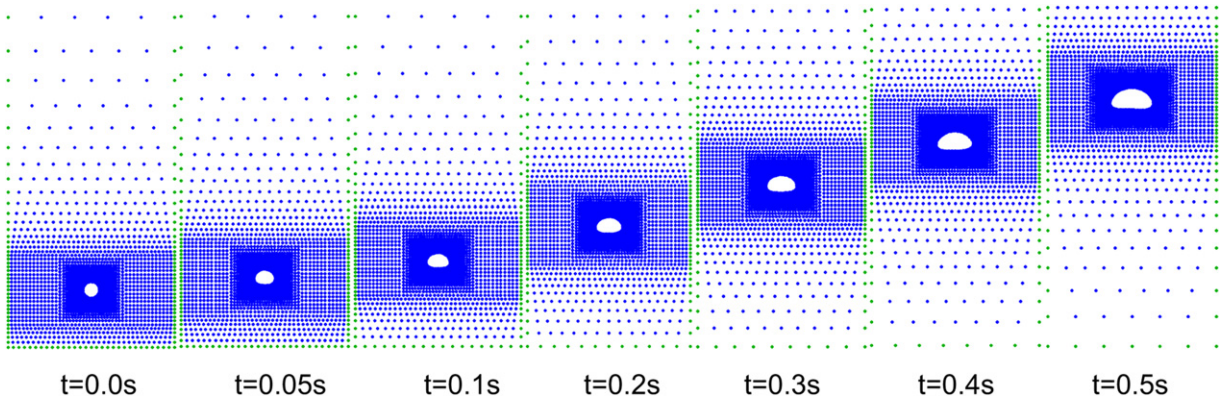

Fig. 15. The bubble rising process in Na with initial diameter 10 mm.

3.2. The bubble rising process in different stagnant liquid metals

The rising process of a single nitrogen bubble with an initial diameter at 10 mm in five kinds of common stagnant liquid metals, namely Na (200 °C), K (200 °C), Na–K (25% Na, 200 °C), Li–Pb (15.7%–16.98% Li, 300 °C) and LBE (56.5% Bi, 200 °C), are also simulated using MPS method, respectively.

As shown in Fig. 13, at about 0.03 s, the rising velocities reach around 0.175 m/s. Then, the rising velocities increase with a fluctuated low speed. The bubble terminal rising velocity in 5 liquid metals is at around 0.23 m/s. The largest bubble terminal rising velocity is 0.25 m/s in these liquid metals.

Table 3 lists the physical properties of liquid and inert gas, as well as bubble dimensionless numbers during the bubble rising process in 5 liquid metals.

Fig. 14 shows Grace's diagram when Eo numbers of bubble rising in K, Na, Na–K, Li–Pb and LBE are 4.78, 7.88, 8.05, 21.10, 29.71, respectively. From Fig. 14, we can see that the bubble final shape in Li–Pb and LBE is similar to spherical cap, while in K, Na, Na–K the bubble final shape is ellipsoid.

Fig. 15 shows the bubble rising behavior in liquid metal Na. From the figure, the bubble terminal shape-elliptical shape, is obtained.

3.3. The bubble rising process in flowing lead bismuth alloy with different liquid velocities

The rising behaviors of the single nitrogen gas bubble in flowing lead bismuth alloy (56.5%Bi, 200 °C), with initial bubble diameter 16 mm, when the liquid velocity is 0.04 m/s, are shown in Fig. 16. The deformation of bubble is similar to the rising behaviors in stagnant lead bismuth alloy with initial bubble diameter 16 mm.

The Fig. 17 shows the bubble aspect ratio changes in different liquid velocities. When the initial bubble diameter is 16 mm, with the liquid velocity increases, the aspect ratio is larger. The terminal aspect ratios are between 0.3 and 0.6.

In Fig. 18, it shows the bubble rising velocity in flowing lead bismuth alloy with different liquid velocities – 0.0 m/s, 0.04 m/s, 0.07 m/s, 0.1 m/s, when the initial bubble diameter is 16 mm. The trend of the bubble rising velocity is similar to the velocity of

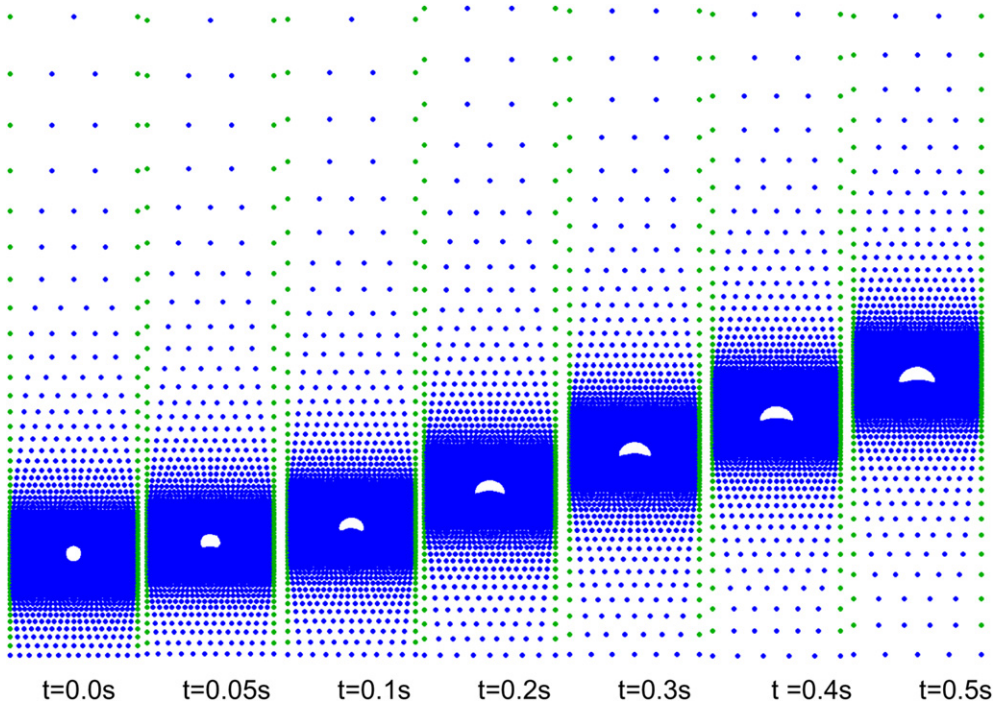

Fig. 16. The bubble rising process in flowing lead bismuth alloy.

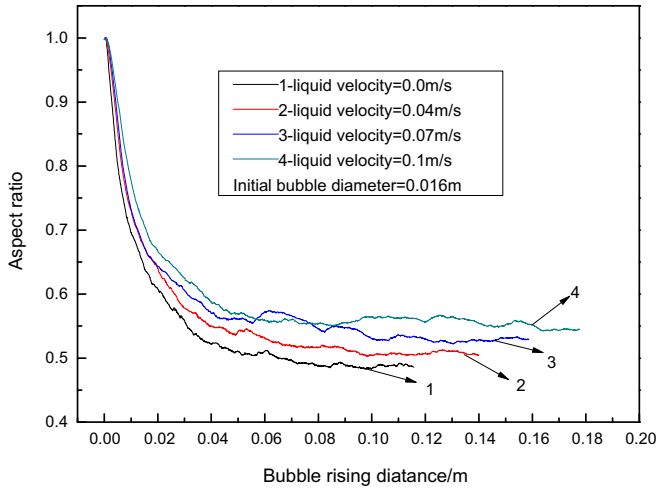

Fig. 17. The bubble aspect ratio in flowing lead bismuth alloy with different liquid velocities.

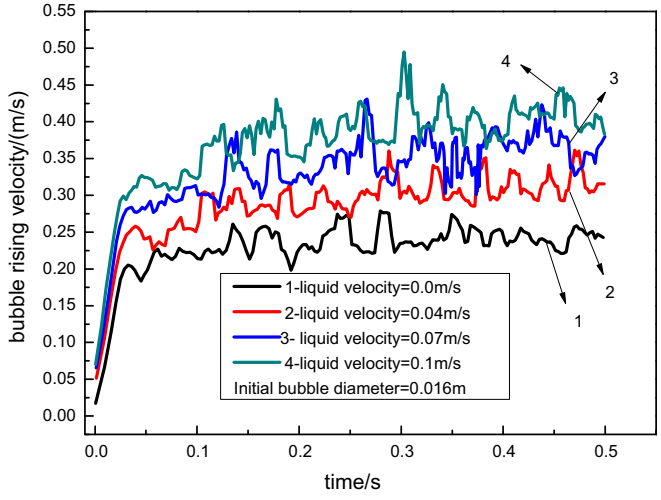

Fig. 18. The bubble rising velocity in flowing lead bismuth alloy with different liquid velocities.

bubble in stagnant liquid, but the terminal velocity is larger obviously. The terminal velocities are between 0.2 m/s and 0.425 m/s.

4. Conclusions

In present study, by using the mesh-free numerical method, MPS, the single nitrogen bubble rising behaviors in stagnant lead bismuth alloy with different initial bubble diameters, in different kinds of stagnant liquid metals and in flowing lead bismuth alloy with different liquid velocities were studied. The liquid phase was modeled using moving particles and the bubble phase was treated using real gas state equation. The two phase interface was captured through the Lagrangian motion of interfacial particles. The key conclusions of the present work are as follows.

(1) In stagnant lead bismuth alloy, the changing processes of the bubble shapes of nitrogen bubble are similar as initial bubble diameter at 10 mm, 16 mm and 20 mm. The bubble shape changes from a sphere to a dimples shape during the rising process, and ultimately develops a spherical crown. The aspect ratio decreases rapidly from 1.0 to the value around 0.5–0.6. The terminal rising velocity of the spherical crown bubble and aspect ratio increase with the increase of the initial bubble diameter. Besides, terminal velocity calculated by MPS has a little difference with the values calculated by empirical correlation.

(2) In all 5 kinds of common stagnant liquid metals, when the initial bubble diameter is 10 mm, the bubble final shape in Li–Pb and LBE is near spherical cap, while in K, Na, Na–K the bubble final shape is ellipsoid. And the terminal velocity does not exceed 0.3 m/s.

(3) In MPS method, the fluid temperature has little influence on the parameters, such as aspect ratio and bubble rising velocity.

(4) In the flowing lead bismuth alloy, when the initial bubble diameter is 16 mm, as the liquid velocity increases, both the bubble aspect ratio and terminal velocity increase as well. The terminal aspect ratios are between 0.3 and 0.6. The terminal velocities are between 0.2 m/s and 0.425 m/s.

(5) MPS method is a valid method to study a single bubble rising behavior in stagnant and flowing liquid metal. The parameters calculated by this method, such as bubble terminal velocity and aspect ratio, have significantly influenced on the mechanism research of two phase flow in liquid metal. And this work will be important to the study of the natural circulation capability of Accelerator Driven System (ADS) by using gas-lift pump.

Acknowledgments

The present study is supported by the National Natural Science Foundation (No. 10905045, 91126009, 11125522) of China and by the doctoral fund for Young Teacher of Ministry of Education (No. 20090201120002) of China.

References

Celata, G.P., D'Annibale, F., Marco, P.D., Memoli, G., Tomiyama, A., 2007. Measurements of rising velocity of a small bubble in a stagnant fluid in one- and two-component systems. Experimental Thermal and Fluid Science 31, 609–623.
Cinotti, L., Gherardi, G., 2002. The Pb–Bi cooled XADS status of development. Journal of Nuclear Materials 301, 11–15.
Clift, R., Grace, J.R., Weber, M.E., 1978. Bubbles, Drops and Particles. Academic Press, New York, p. 172.
Dhotre, M.T., Smith, B.L., 2007. CFD simulation of large-scale bubble plumes: comparisons against experiments. Chemical Engineering Science 62, 6615–6630.
Duan, R.Q., Koshizuka, S., Oka, Y., 2003. Two-dimensional simulation of drop deformation and breakup at around the critical Weber number. Nuclear Engineering and Design 225, 37–48.
Grace, J.R., 1973. Shapes and velocities of bubbles rising in infinite liquids. Transactions of the Institution of Chemical Engineering 51, 116–120.
Grace, J.R., 1976. Shapes and velocities of single drops and bubbles moving freely through immiscible liquids. Transactions of the Institution of Chemical Engineering 54, 167–173.
Heo, S., Koshizuka, S., Oka, Y., 2002. Numerical analysis of boiling on high heat-flux and high subcooling condition using MPS-MAFL. International Journal of Heat and Mass Transfer 45, 2633–2642.
Koshizuka, S., Oka, Y., 1996. Moving-particle semi-implicit method for Fragmentation of incompressible fluid. Nuclear Science and Engineering 123, 421–434.
Levich, V.G., 1972. Physicochemical Hydrodynamics. Prentice-Hal, New York.
Marco, P.D., Grassi, W., Memoli, G., 2003. Experimental study on rising velocity of nitrogen bubbles in FC-72. International Journal of Thermal Sciences 42, 435–446.
Mikityuk, K., Vasiliev, A., Fomichenko, P., Alekseev, P., 2002. Safety parameters of advanced RBEC-M Lead–Bismuth cooled fast reactor. In: Proc. Int. Conf. on the New Frontiers of Nuclear Technology: Reactor Physics, Safety and High Performance Computing, Seoul, Korea.
Peebles, F., Garber, H., 1953. Studies on the motion of gas bubbles in liquid. Chemical Engineering Progress 49, 88–97.
Scardovelli, R., Zaleski, S., 1999. Direct numerical simulation of free-surface and interfacial flow. Annual Review of Fluid Mechanics 31, 567–603.
Schlichting, H., 1979. Boundary-layer Theory, seventh ed. McGraw-Hill, New York, p. 116.
Smereka, P., Sethian, J.A., 2003. Level set methods for fluid interfaces. Annual Review of Fluid Mechanics 35, 341–372.
Suzuki, T., Tobita, Y., Kondo, S., Saito, Y., Mishima, K., 2003. Analysis of gas–liquid metal two-phase flows using a reactor safety analysis code SIMMER-III. Nuclear Engineering and Design 220, 207–223.

Tian, W., Ishiwatari, Y., Ikejiri, S., Yamakawa, M., Oka, Y., 2009. Numerical simulation on void bubble dynamics using moving particle semi-implicit method. Nuclear Engineering and Design 239, 2382–2390.

Tian, W., Ishiwatari, Y., Ikejiri, S., Yamakawa, M., Oka, Y., 2010. Numerical computation of thermally controlled steam bubble condensation using moving particle semi-implicit(MPS) method. Annals of Nuclear Energy 37, 5–15.

Tohru, S., Xue-Nong, C.I.R.A., Werner, M., 2005. Transient analyses for accelerator driven system PDS-XADS using the extended SIMMER-III code. Nuclear Engineering and Design 235, 2594–2611.

Tomiyama, A., Kataoka, I., Zun, I., Sakaguchi, T., 1998. Drag coefficients of single bubbles under normal and microgravity conditions. JSME International Journal Series D 41, 472–479.

Unverdi, O., Tryggvason, G., 1992. A front-tracking method for viscous, incompressible, multi-fluid flows. Journal of Computational Physics 100, 25–37.

Yoon, H.Y., Koshizuka, S., Oka, Y., 1999. A mesh-free numerical method for direct Simulation of gas–liquid phase interface. Nuclear Science and Engineering 133, 1–9.